Available online at www.sciencedirect.com

ScienceDirect

Mendeleev Commun., 2021, **31**, 462–464

Mendeleev Communications

Simple *in situ* analysis of metal halide perovskite-based sensor materials using micro X-ray fluorescence and inductively coupled plasma mass spectrometry

Egor A. Eliseev, Daria G. Filatova,* Artem S. Chizhov, Marina N. Rumyantseva and Alexander M. Gaskov

Department of Chemistry, M. V. Lomonosov Moscow State University, 119991 Moscow, Russian Federation.
E-mail: gak1.analyt@gmail.com

DOI: 10.1016/j.mencom.2021.07.008

A new approach to *in situ* analysis of the composition of photosensitive metal halide perovskite-based materials for gas sensor has been developed. The concentration of Cs, Pb, Br and I in the ZnO layer was determined by *in situ* micro X-ray fluorescence method using inductively coupled plasma mass spectrometry for calibration. The relationship 'synthesis conditions–composition–photoresponse' of the sensor has been established based on the results obtained.

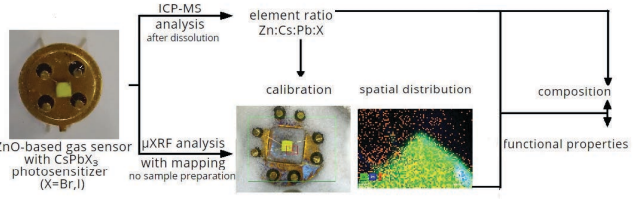

Keywords: halide perovskites, characterization, micro-XRF, mapping, ICP-MS, ZnO/$CsPbBr_3$, ZnO/$CsPbI_3$.

Metal halide perovskites are described by the general formula ABX_3, where A is an alkali metal cation (for example, Cs), B is a divalent metal cation (most often Pb or Sn) and X is a halide anion (Cl, Br, I). Such compounds are widely used in optoelectronics and photovoltaics. Metal halide perovskites have shown great potential in photovoltaic and optoelectronic devices due to their luminescence, characterized by high brightness, defect tolerance, tunable emission wavelength, high color purity and increased quantum yield.[1–4] The combination of light absorption in the visible region, a high-located excited energy level and suppressed nonradiative recombination of photoexcited electron–hole pairs makes nanocrystals of lead halide perovskites promising materials for use in light-emitting devices,[5] solar cells,[6] ionizing radiation detectors[7] and visible light-activated semiconductor gas sensors.[8] It has been shown[9–13] that the gas sensitivity of semiconductor metal oxides can be activated by ultraviolet radiation at room temperature without additional heating, which is a promising way to reduce the energy consumption of semiconductor gas sensors. Increasing sensitivity of sensor materials to visible light is usually achieved by combining wide-band metal oxides with photosensitizers such as organic dyes or semiconductor quantum dots.[8,14–21]

The optical properties of photosensitive materials based on wide-band oxides and semiconductor quantum dots strongly depend on the photosensitizer composition and the photosensitizer/semiconductor matrix ratio.[14] It is known[1,22] that significant deviations from the stoichiometric ratio Cs : Pb = 1 : 1 in cesium lead halides $CsPbX_3$ result in a high density of donor or acceptor states in the band gap of $CsPbX_3$ due to the appearance of various point defects. These effects ultimately lead to the weakening and broadening of spectral lines.[23] At the same time, the use of solid solutions $CsPbCl_{3-x}Br_x$ and $CsPbBr_{3-x}I_x$ makes it possible to accurately control the absorption and photoluminescence spectra in the range of 400–700 nm.[24] For the development and scalable production of light-activated gas sensors, it is necessary to conduct a non-destructive analysis of the composition of the sensitive layer containing the photosensitizer on a ready-to-use sensor. Such an analysis is non-trivial and requires the development of specific analytical procedures.

Therefore, it is necessary to develop approaches for the reliable *in situ* determination of the composition of $CsPbX_3$ nanocrystals and their distribution over the surface of a ready-to-use sensor layer to establish the 'composition–functional properties' relationship. Energy-dispersive X-ray analysis is commonly used to characterize new materials.[25–27] However, the accuracy of this method can depend on various factors such as sample surface morphology and matrix composition. Some of them can be taken into account if certified reference samples are available, but there are no such samples for new materials. Total reflection X-ray fluorescence spectroscopy has recently been proposed to determine the bulk composition of lead halide perovskite nanocrystals.[28] Nevertheless, this method is inconvenient for *in situ* analysis because the ready-to-use sensor's sample preparation is required. X-ray fluorescence is a widespread analytical method for determining the elemental composition of bulk materials. However, nowadays, with focusing optics available, micro X-ray fluorescence (micro-XRF) can also be performed with laboratory instruments. The advantage of the new micro-XRF technique is the fast, high-resolution analysis of element distribution.[29] For example, the uniformity of the Cs : Pb ratio has been proven by micro-XRF mapping over the entire surface of a $CsPbBr_3$ crystal deposited on a platinum electrode.[30]

In this work, we propose a novel approach to the chemical characterization of ZnO–$CsPbBr_3$ and ZnO–$CsPbI_3$ materials deposited on a microelectronic chip. The approach is based on a modern high-sensitivity version of micro-XRF† for determining the distribution of metal halide perovskites on the surface of a ready-to-use sensor and quantifying Cs, Pb, Hal and Zn. The method of inductively coupled plasma mass spectrometry (ICP-MS)† was developed to analyze ZnO–

† For details, see Online Supplementary Materials.

$CsPbBr_3$ and ZnO–$CsPbI_3$ powders and is used as a reference analytical technique for verifying results obtained by the micro-XRF method in the absence of standard reference samples.

ZnO–$CsPbBr_3$ samples were prepared† and analyzed by the ICP-MS method. According to the published data, the quantitative determination of Cs, Pb and Br is possible separately in acidic solutions without any cross interference using the ICP-MS method.[31,32] The quantification of bromide in an acidic medium by ICP-MS is reported to have high quantification limits. The reason for this is polyatomic interferences: the $^{40}Ar_2{}^1H^+$ signal overlaps with the ^{81}Br signal, and the $^{40}Ar^{38}Ar^1H^+$ signal overlaps with ^{79}Br.[33,34] We have checked the validity of the results using the 'introduced–found' method since the simultaneous determination of Cs, Pb and Br by the ICP-MS method had not been previously described. The results are shown in Table S1.

The synthesized perovskite compounds and the sensitive layer of the ready-to-use sensor were analyzed separately after dissolution. $CsPbBr_3$ quantum dots with a hydrophobic shell were dissolved in DMF, and then in 2% HNO_3. The active layer of the sensor was dissolved in HNO_3. The results are shown in Table S2. More than the expected amount of bromide was found in the material. The $CsPbBr_x$ sample may be contaminated with Br^- during the synthesis. Therefore, to obtain the desired stoichiometry, additional purification of the sample from excess bromide ion is required. We have shown that additional purification by recrystallization from a non-polar solvent makes it possible to obtain a material of a certain composition. The composition of $CsPbBr_x$ in the ZnO matrix of the sensor's sensitive layer was determined with a relative standard deviation of 0.05, 0.03 and 0.07 for Cs, Pb and Br, respectively. We can assume the existence of a pure $CsPbBr_3$ phase since the Cs : Pb ratio has been proven to be 1 : 1. It has been found that accurate simultaneous quantification of Cs, Pb and Br is possible using 2% HNO_3.

The analysis of ZnO–$CsPbI_3$ samples† turned out to be more complicated compared to their bromo analogs. According to the known data, the iodide ion determination in an acidic medium is impossible due to HI formation. Therefore, alkaline solutions of NaOH and tetramethylammonium hydroxide (TMAH) were used for determination.[35,36] The results of the simultaneous determination of Cs, Pb and I in model solutions of 0.4% NaOH and 2% TMAH by ICP-MS are presented in Table S3. We noticed the loss of Pb in the NaOH solution, which is probably associated with the precipitation of hydroxide, and the loss of I^- due to possible disproportionation. It was impossible to account for the lead loss in NaOH solution even when using an adequate reference solution for calibration. An increase in NaOH concentration to 2% for forming a soluble lead complex also did not reduce the analyte loss. Nevertheless, in the TMAH solution, we were able to determine all the elements accurately. The probable reason for this is the formation of an ionic associate of the TMAH cation with iodide.[37] Besides, in this case, the concentration of OH^- ions is sufficient for the formation of Pb^{II} hydroxo complexes. The use of TMAH solution may reduce the limit of quantification for analytes reaching C_{lim} values of 0.5, 0.1 and 5 ppb for Cs, Pb and I, respectively. The results of the analysis of a ready-to-use sensor in the TMAH solution are presented in Table S4. Stoichiometry of $CsPbI_{3.3}$ has been established in the sensitive layer of the sensor. We attribute the excessive amount of iodide to contamination during synthesis.

The distribution of elements in the sensitive layer of the ready-to-use sensor was analyzed using micro-XRF mapping without sample preparation (Figure 1). For this, the sensor was placed in dry boric acid to reduce the background effect. The data obtained demonstrate that Zn, Cs, Pb, Br and I are distributed over the sensor surface slightly unevenly (Figure 2). The excess

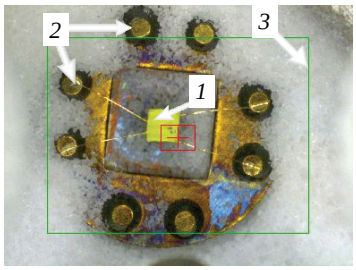

Figure 1 Photograph of a ZnO/$CsPbBr_3$ sensor consisting of (*1*) a sensitive layer and (*2*) contacts, which was placed in (*3*) boric acid for micro-XRF measurements.

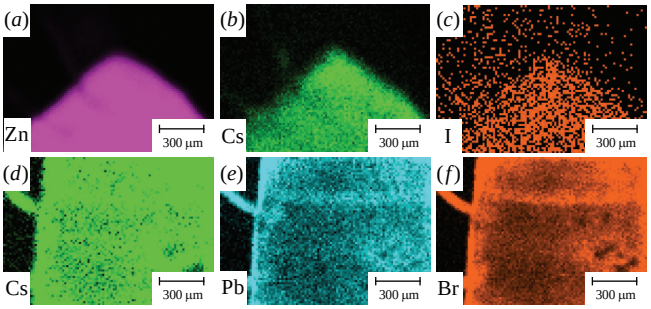

Figure 2 Element distribution maps of sensitive layers in the ZnO/$CsPbI_3$ sensor for (*a*) Zn, (*b*) Cs and (*c*) I and in the ZnO/$CsPbBr_3$ sensor for (*d*) Cs, (*e*) Pb and (*f*) Br.

amount of iodide was detected by the ICP-MS method and was obviously caused by iodine impurities in the substrate used to prepare the perovskite compound [Figure 2(*c*)]. The characteristic Pt L_2–M_4 lines in the spectra are induced by wire material emission. Fe and Ni contaminants indicated by the emerging emission of the Fe K–L_3 and Ni K–M_3 lines were probably visualized due to the fluorescence of the sensor base material [Figures 3(*a*),(*b*)]. The composition of the sensitive layer can be determined using point spectra instead of mapping in the case of a uniform distribution of the perovskite compound.

The results of element quantification by ICP-MS in sample solutions after decomposition were used once as an external standard for micro-XRF results. Then the obtained coefficients were used for calculations. To solve this complex problem, we proposed the following approach. We used only four samples with different content of $CsPbX_3$ quantum dots (QDs) to calibrate the results of micro-XRF because the ratio of elements in the sample is almost constant, and their content changes synchronously with an increase in the concentration of QDs. For the elements of each sample, the correlation coefficients with the ICP-MS results (atomic moles, *n*) are calculated from the areas of the corresponding micro-XRF peaks after their normalization to the Cs peak intensity. We assume that the samples have the same thickness since the Cs peak intensity is approximately proportional to its content in the sensor layer. The conversion

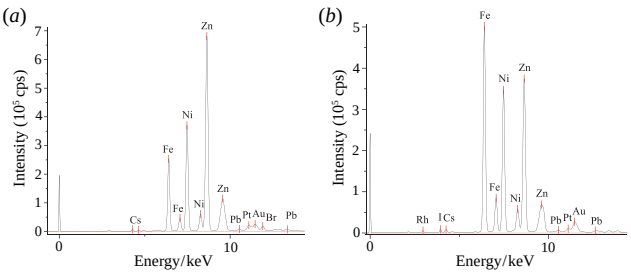

Figure 3 XRF spectra of the sensor surfaces consisting of (*a*) ZnO/$CsPbBr_3$ and (*b*) ZnO/$CsPbI_3$.

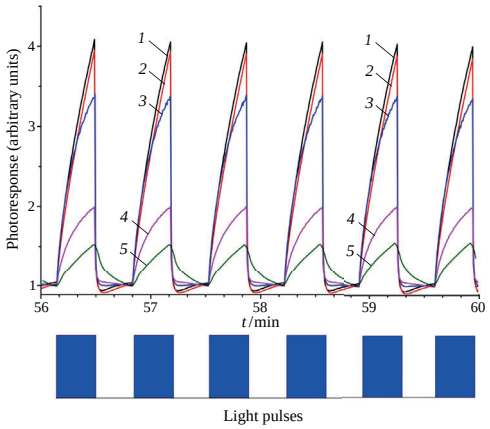

Figure 4 Photoresponse (σ/σ_{dark}) of (*1*)–(*4*) ZnO/$CsPbBr_3$ sensors with different $CsPbBr_3$ content ($c_1 > c_2 > c_3 > c_4$) and (*5*) non-sensitized ZnO under blue light illumination (λ_{max} = 470 nm, 8 mW cm^{-2}) in air.

coefficients *k* were found to converge within an error of 10% for different contents of QD elements. We noted that applying the fundamental parameter approach to calculating element ratios leads to incorrect results for such samples. Substance amounts (atomic moles, *n*) were calculated for the micro-XRF results as (normalized peak area) × *k*.† The proposed approach allowed for rapid *in situ* chemical characterization of sensors using micro-XRF to establish the 'composition–properties' relationship.

The proposed approach was used to determine the composition of ZnO/$CsPbBr_3$ composites *in situ* using non-destructive micro-XRF analysis and investigate the 'composition–functional properties' relationship (Figure 4). It was found that the photoconductivity of ready-to-use sensors under visible light exposure depends on the $CsPbBr_3$ concentration in the ZnO/$CsPbBr_3$ sensitive layer.

Thus, a novel approach to the *in situ* chemical characterization of sensors based on metal halide perovskite compounds is proposed. The approach involves a combination of micro-XRF with mapping and ICP-MS in solutions after sample decomposition. The mapping function visualized the distribution of components over the sensor surface, and its partial uniformity was established. The data obtained by ICP-MS was used to quantify Zn, Cs, Pb, Br and I in the ZnO matrix, confirm $CsPbBr_3$/$CsPbI_3$ stoichiometry and calculate coefficients for quantitative micro-XRF analysis in the absence of reference samples. The method for quantitative calculation of X-ray fluorescence analysis data is based on statistical correlation with the ICP-MS results. It is pretty simple and does not require any additional tools. It is noted that using the method of fundamental parameters leads to incorrect quantitative results.

This work was supported by the Russian Foundation for Basic Research (grant no. 18-33-01004) with the use of equipment purchased on behalf of the Development Program of M. V. Lomonosov Moscow State University.

Online Supplementary Materials

Supplementary data associated with this article can be found in the online version at doi: 10.1016/j.mencom.2021.07.008.

References

1 L. Protesescu, S. Yakunin, M. I. Bodnarchuk, F. Krieg, R. Caputo, C. H. Hendon, R. X. Yang, A. Walsh and M. V. Kovalenko, *Nano Lett.*, 2015, **15**, 3692.
2 H. Zhao, Y. Zhou, D. Benetti, D. Ma and F. Rosei, *Nano Energy*, 2017, **37**, 214.
3 H. Chen, A. Guo, J. Zhu, L. Cheng and Q. Wang, *Appl. Surf. Sci.*, 2019, **465**, 656.
4 E. I. Marchenko, S. A. Fateev, A. A. Petrov, E. A. Goodilin and A. B. Tarasov, *Mendeleev Commun.*, 2020, **30**, 279.
5 Y.-F. Li, J. Feng and H.-B. Sun, *Nanoscale*, 2019, **11**, 19119.
6 P. Tonui, S. O. Oseni, G. Sharma, Q. Yan and G. T. Mola, *Renewable Sustainable Energy Rev.*, 2018, **91**, 1025.
7 H. Wei and J. Huang, *Nat. Commun.*, 2019, **10**, 1066.
8 A. S. Chizhov, M. N. Rumyantseva, K. A. Drozdov, I. V. Krylov, M. Batuk, J. Hadermann, D. G. Filatova, N. O. Khmelevsky, V. F. Kozlovsky, L. N. Maltseva and A. M. Gaskov, *Sens. Actuators, B*, 2021, **329**, 129035.
9 E. Espid and F. Taghipour, *Crit. Rev. Solid State Mater. Sci.*, 2017, **42**, 416.
10 J. Wang, H. Shen, Y. Xia and S. Komarneni, *Ceram. Int.*, 2021, **47**, 7353.
11 F. Xu and H.-P. HO, *Micromachines*, 2017, **8**, 333.
12 R. Kumar, X. Liu, J. Zhang and M. Kumar, *Nano-Micro Lett.*, 2020, **12**, 164.
13 A. Chizhov, M. Rumyantseva and A. Gaskov, *Nanomaterials*, 2021, **11**, 892.
14 A. Chizhov, R. Vasiliev, M. Rumyantseva, I. Krylov, K. Drozdov, M. Batuk, J. Hadermann, A. Abakumov and A. Gaskov, *Frontiers in Materials*, 2019, **6**, 231.
15 M. Ekrami, G. Magna, Z. Emam-djomeh, M. Saeed Yarmand, R. Paolesse and C. Di Natale, *Sensors*, 2018, **18**, 2279.
16 M. Rumyantseva, A. Nasriddinov, S. Vladimirova, S. Tokarev, O. Fedorova, I. Krylov, K. Drozdov, A. Baranchikov and A. Gaskov, *Nanomaterials*, 2018, **8**, 671.
17 C. Zhang, J. Wang, M.-G. Olivier and M. Debliquy, *Sens. Actuators, B*, 2015, **209**, 69.
18 E. V. Lukovskaya, O. A. Fedorova, Yu. A. Glazova, Yu. V. Fedorov, A. V. Anisimov, E. V. Podolko, M. N. Rumyantseva, A. M. Gaskov and F. Fages, *Organic Photonics and Photovoltaics*, 2015, **3**, 54.
19 A. S. Chizhov, M. N. Rumyantseva, R. B. Vasiliev, D. G. Filatova, K. A. Drozdov, I. V. Krylov, A. V. Marchevsky, O. M. Karakulina, A. M. Abakumov and A. M. Gaskov, *Thin Solid Films*, 2016, **618**, 253.
20 A. S. Chizhov, N. E. Mordvinova, M. N. Rumyantseva, I. V. Krylov, K. A. Drozdov, X. Li and A. M. Gas'kov, *Russ. J. Inorg. Chem.*, 2018, **63**, 512 (*Zh. Neorg. Khim.*, 2018, **63**, 480).
21 R. Chen, J. Wang, Y. Xia and L. Xiang, *Sens. Actuators, B*, 2018, **255**, 2538.
22 C.-Y. Chen, H.-Y. Lin, K.-M. Chiang, W.-L. Tsai, Y.-C. Huang, C.-S. Tsao and H.-W. Lin, *Adv. Mater.*, 2017, **29**, 1605290.
23 S. Seth, T. Ahmed, A. De and A. Samanta, *ACS Energy Lett.*, 2019, **4**, 1610.
24 L. B. Matyushkin and V. A. Moshnikov, *Semiconductors*, 2017, **51**, 1337 (*Fiz. Tekh. Poluprovodn.*, 2017, **51**, 1387).
25 X. Du, G. Wu, J. Cheng, H. Dang, K. Ma, Y.-W. Zhang, P.-F. Tan and S. Chen, *RSC Adv.*, 2017, **7**, 10391.
26 T. Paul, B. K. Chatterjee, N. Besra, S. Thakur, S. Sarkar and K. K. Chattopadhyay, *Mater. Today: Proc.*, 2018, **5**, 2234.
27 C.-H. Tien, L.-C. Chen, K.-Y. Lee, Z.-L. Tseng, Y.-S. Dong and Z.-J. Lin, *Energies*, 2019, **12**, 3507.
28 I. Allegretta, R. Giannelli, R. Grisorio, G. P. Suranna and R. Terzano, *Spectrochim. Acta, Part B*, 2020, **164**, 105750.
29 M. Haschke, *Laboratory Micro-X-Ray Fluorescence Spectroscopy: Instrumentation and Applications*, Springer, Cham, 2014.
30 X. Li, Y. Luo, M. V. Holt, Z. Cai and D. P. Fenning, *Chem. Mater.*, 2019, **31**, 2778.
31 S. M. Enamorado-Báez, J. M. Abril and J. M. Gómez-Guzmán, *ISRN Anal. Chem.*, 2013, 851713.
32 S. Takahashi, I. Takahashi, H. Sato, Y. Kubota, S. Yoshida and Y. Muramatsu, *Lab. Anim.*, 2000, **34**, 97.
33 H. Balcone-Boissard, A. Michel and B. Villemant, *Geostand. Geoanal. Res.*, 2009, **33**, 477.
34 L. Xu, C. Luo, H. Ling, Y. Tang and H. Wen, *Int. J. Mass Spectrom.*, 2018, **432**, 52.
35 K. Brix, C. Hein, J. M. Sander and R. Kautenburger, *Talanta*, 2017, **167**, 532.
36 M. Haldimann, A. Eastgate and B. Zimmerli, *Analyst*, 2000, **125**, 1977.
37 S. A. Steiner, D. M. Watson and J. S. Fritz, *J. Chromatogr. A*, 2005, **1085**, 170.

Received: 4th March 2021; Com. 21/6480